



HAL
open science

Unsymmetrical binding modes of the HOPNO inhibitor of tyrosinase: from model complexes to the enzyme

Constance Bochot, Elisabeth Favre, Carole Dubois, Benoît Baptiste, Luigi Bubacco, Pierre-Alain Carrupt, Gisèle Gellon, Renaud Hardré, Dominique Luneau, Yohann Moreau, et al.

► To cite this version:

Constance Bochot, Elisabeth Favre, Carole Dubois, Benoît Baptiste, Luigi Bubacco, et al.. Unsymmetrical binding modes of the HOPNO inhibitor of tyrosinase: from model complexes to the enzyme. *Chemistry*, 2013, 19 (11), pp.3655-3664. 10.1002/chem.201202643 . hal-01107636

HAL Id: hal-01107636

<https://hal.science/hal-01107636v1>

Submitted on 7 Oct 2022

HAL is a multi-disciplinary open access archive for the deposit and dissemination of scientific research documents, whether they are published or not. The documents may come from teaching and research institutions in France or abroad, or from public or private research centers.

L'archive ouverte pluridisciplinaire **HAL**, est destinée au dépôt et à la diffusion de documents scientifiques de niveau recherche, publiés ou non, émanant des établissements d'enseignement et de recherche français ou étrangers, des laboratoires publics ou privés.



Distributed under a Creative Commons Attribution - NonCommercial 4.0 International License

Unsymmetrical Binding Modes of the HOPNO Inhibitor of Tyrosinase: From Model Complexes to the Enzyme

Constance Bochot,^[a] Elisabeth Favre,^[b] Carole Dubois,^[c] Benoit Baptiste,^[a]
Luigi Bubacco,^[d] Pierre-Alain Carrupt,^[b] Gisèle Gellon,^[a] Renaud Hardré,^[c]
Dominique Luneau,^[e] Yohann Moreau,^[f] Alessandra Nurisso,^[b] Marius Réglie,^[c]
Guy Serratrice,^[a] Catherine Belle,^{*,[a]} and Hélène Jamet^{*,[a]}

Abstract: The deciphering of the binding mode of tyrosinase (Ty) inhibitors is essential to understand how to regulate the tyrosinase activity. In this paper, by combining experimental and theoretical methods, we studied an unsymmetrical tyrosinase functional model and its interaction with 2-hydroxypyridine-*N*-oxide (HOPNO), a new and efficient competitive inhibitor for bacterial Ty. The tyrosinase model

was a dinuclear copper complex bridged by a chelated ring with two different complexing arms (namely (bis(2-ethylpyridyl)amino)methyl and (bis(2-methylpyridyl)amino)methyl). The geometrical asymmetry of the complex induces

Keywords: bioinorganic chemistry • copper • density functional calculations • enzymes • inhibitors

an unsymmetrical binding of HOPNO. Comparisons have been made with the binding modes obtained on similar symmetrical complexes. Finally, by using quantum mechanics/molecular mechanics (QM/MM) calculations, we studied the binding mode in tyrosinase from a bacterial source. A new unsymmetrical binding mode was obtained, which was linked to the second coordination sphere of the enzyme.

Introduction

Tyrosinases (Tys, EC 1.14.18.1) are copper-containing enzymes belonging to the type-3 family or coupled binuclear family.^[1] Three distinct forms have been identified in various stages of the catalytic cycle: a native met state (Cu^{II}–Cu^{II}) bridged by aquo (hydroxo) ligands, a reduced deoxy state (Cu^I Cu^I), and an oxy state with a dioxygen molecule bound to the dicopper center (Cu^{II}–O₂²⁻–Cu^{II}).^[2] Tys are present in almost all types of organism^[3] and their main function is pigment biosynthesis. In mammals, Ty is responsible for the critical steps in eumelanin production (the most protective melanin, found particularly in the skin).^[4] Melanin-related disorders are known to cause serious skin lesions^[5] and melanoma,^[6] and Parkinson's disease has been linked to Ty,^[7] so this enzyme family has considerable interest for medicinal chemistry. In fungi and plants, Ty catalyzes the oxidation of phenolic compounds and subsequently produces types of melanins called allomelanins.^[8] In the area of food storage, Ty is a key enzyme in the browning process that occurs upon tissue damage or long storage. For these reasons, a large variety of synthetic or natural compounds have been tested as Ty inhibitors.

A large number of the Ty inhibitors described in the literature target the Ty binuclear copper active site. These inhibitors, named transition-state (TS) analogues, are structural analogues of catechol but cannot be oxidized. Kojic acid^[9] (5-hydroxy-2-(hydroxymethyl)-4-pyrone, KA) and HOPNO^[10] (2-hydroxypyridine-*N*-oxide) are good paradigms of this strategy. The binding mode of these inhibitors

[a] Dr. C. Bochot, Dr. B. Baptiste, G. Gellon, Prof. G. Serratrice, Dr. C. Belle, Dr. H. Jamet
Département de Chimie Moléculaire
Equipes CIRe et Chimie Théorique
Université J. Fourier, UMR-CNRS 5250, ICMG FR-2607
BP 53, 38041, Grenoble, Cedex 09 (France)
Fax: (+33)476-514-836
E-mail: catherine.belle@ujf-grenoble.fr
helene.jamet@ujf-grenoble.fr


[b] Dr. E. Favre, Prof. P.-A. Carrupt, Dr. A. Nurisso
School of Pharmaceutical Sciences
University of Geneva, University of Lausanne
1211 Geneva (Switzerland)

[c] Dr. C. Dubois, Dr. R. Hardré, Dr. M. Réglie
Institut des Sciences Moléculaires de Marseille, équipe Biosciences
Aix Marseille Université, CNRS, ISM2, UMR 7313
13397, Marseille, Cedex 20 (France)

[d] Prof. L. Bubacco
Department of Biology, University of Padova
Via Ugo Bassi 58b, 35121 Padova (Italy)

[e] Prof. D. Luneau
Laboratoire des Multimatériaux et Interfaces UMR-CNRS 5615
Université Claude Bernard Lyon 1, Campus de la Doua
69622 Villeurbanne (France)

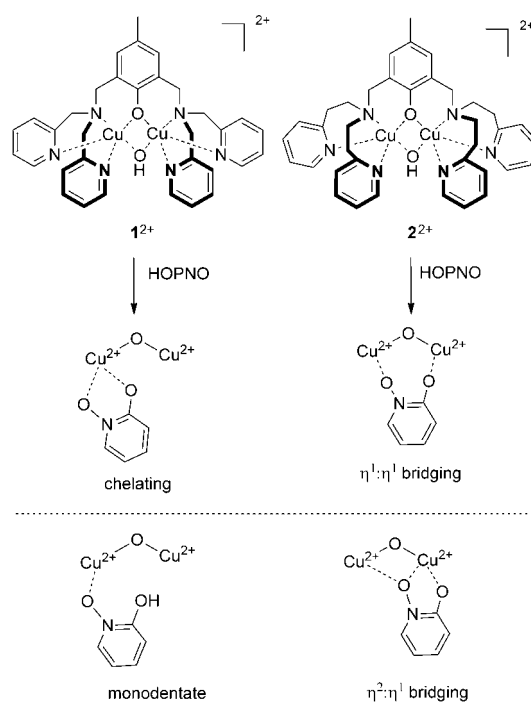
[f] Dr. Y. Moreau
iRTSV/CBM/MCT, CEA Grenoble, 17 avenue des martyrs
38054, Grenoble, Cedex 09 (France)

 Supporting information for this article is available on the WWW under <http://dx.doi.org/10.1002/chem.201202643>.

on the Ty bimetallic center remains an open question. X-ray absorption spectroscopy (XAS), paramagnetic NMR spectroscopy, and electron spin echo envelope modulation (ESEEM) studies suggest direct binding to the copper ions for KA in the adduct with bacterial *Streptomyces antibioticus* Ty, with a $\mu\text{-}\eta^2\text{:}\eta^1$ binding mode reported.^[11] On the other hand, the X-ray crystal structure of the bacterial *Bacillus megaterium* Ty with KA as a ligand reveals that the KA is not bound to the dicopper(II) center but is located at a distance of 7 Å from it.^[2b] Recently, the crystal structure of *Agaricus bisporus* mushroom Ty (deoxy state) in complex with tropolone,^[12] another TS-analogue inhibitor, revealed that tropolone binds near the binuclear copper site without directly coordinating the copper ions. A first approach to obtain more insight into the binding mode is to study inhibitor interactions with low-molecular-weight binuclear copper systems that mimic the dicopper(II) center of the enzyme. To date, few relevant structures with a coordinated inhibitor (or inactivated substrate) have been published.^[13] In particular, there is no example characterized by X-ray analysis in which the various coordination modes of the inhibitor, including an unsymmetrical bridging mode, are described. Recently, we have successfully isolated and fully characterized two 1:1 adducts between the dinuclear copper(II) complexes $[\text{Cu}_2(\text{BPMP})(\mu\text{-OH})](\text{ClO}_4)_2$ (**1**; HBPMP: 2,6-bis[bis(2-pyridylmethyl)-aminomethyl]-4-methylphenol)^[14] and $[\text{Cu}_2(\text{BPEP})(\mu\text{-OH})](\text{ClO}_4)_2$ (**2**; HBPEP: 2,6-bis[bis(2-pyridylethyl)aminomethyl]-4-methylphenol),^[15] known as functional models for Ty catecholase activity, and deprotonated HOPNO. In the first adduct, **1**-OPNO, it binds only one copper(II) atom of the dinuclear site in a chelating mode, but in the second adduct, **2**-OPNO, the inhibitor binds the two copper(II) atoms in a symmetric $\eta^1\text{:}\eta^1$ bridging mode (Scheme 1).

Important information provided by the recent structure resolutions of various Ty forms is the dissymmetry of the active-site structure. The Ty active site is not symmetric and it is composed of two copper atoms, each coordinated by three histidine residues. This dissymmetry is clear in the structure of a met form of the bacterial *S. castaneoglobisporus* Ty (Figure 1; PDB code: 2AHK),^[2a] in which the geometry around the CuA center is close to a square pyramid ($\tau=0.22$), whereas the geometry around the CuB center is intermediate between a square pyramid and a trigonal bipyramid ($\tau=0.48$); ($\tau=0$ for a regular square pyramid and $\tau=1$ for the regular trigonal bipyramid geometry).^[16]

In order to mimic this dissymmetry, we pursued our investigations by generating an unsymmetrical complex, $[\text{Cu}_2(\text{BPMEP})(\mu\text{-OH})](\text{ClO}_4)_2$ (**3**), which was obtained from the new unsymmetrical 2-[bis(2-pyridylethyl)-aminomethyl]-6-[bis(2-pyridylmethyl)-aminomethyl]-4-methylphenol (HBPMEP) ligand (Scheme 2).^[17] The HBPMEP ligand involves two different complexing arms (namely bis(2-ethylpyridyl)amino)methyl and bis(2-methylpyridyl)amino)methyl) in mode to tune an unsymmetrical binding of HOPNO. By combining experimental and theoretical studies, the different complexes and HOPNO binding modes are com-



Scheme 1. Schematic representation of the relevant dicopper model complexes $[\text{Cu}_2(\text{BPMP})(\mu\text{-OH})](\text{ClO}_4)_2$ (**1**)^[14] and $[\text{Cu}_2(\text{BPEP})(\mu\text{-OH})](\text{ClO}_4)_2$ (**2**)^[15] and the characterized or possible binding modes for HOPNO at the dicopper(II) centers.

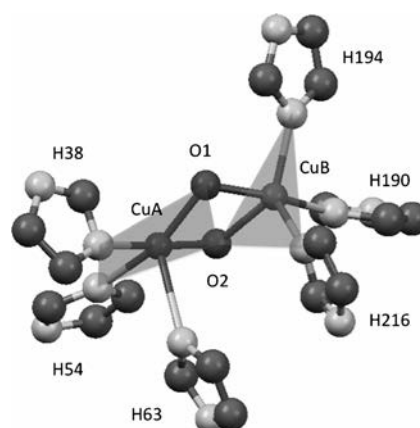
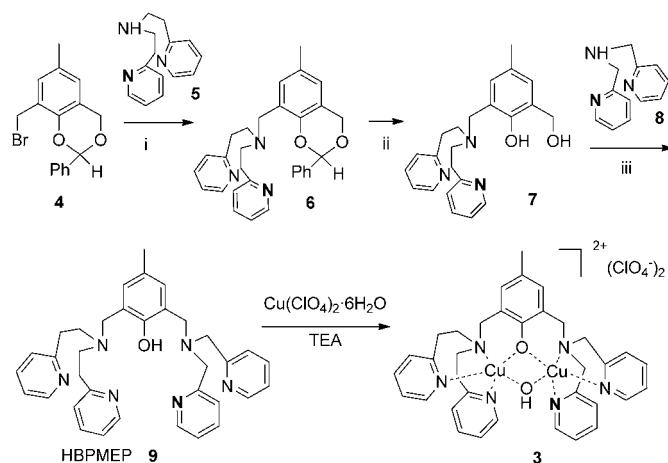


Figure 1. Graphical representation of the met form of the bacterial *Streptomyces castaneoglobisporus* Ty active site (PDB code: 2AHK)^[2a] showing the dissymmetry of the coordination of the two copper centers.

pared. The aim was to get insights into inhibitor binding through variation in the side arms of the dicopper model complexes. Finally, adducts found with model complexes were used to study the binding mode of HOPNO on bacterial Ty by computational methods. We choose bacterial Ty because crystallographic structures of the met form have only been obtained for this tyrosinase and the met form corresponds to the electronic structure of our model complexes ($\text{Cu}^{\text{II}}\text{-Cu}^{\text{II}}$). A hybrid quantum mechanics (QM/MM) method combining classical MM and a QM method was employed on the whole enzyme. The results obtained highlight



Scheme 2. Synthesis of the HBPMEP ligand (**9**) and complex **3**: i) *N,N*-bis(2-ethylpyridyl)amine (**5**), 54%; ii) HBF_4 (48% in water/MeCN), 90%; iii) 1) SOCl_2 , 2) *N,N*-bis(2-methylpyridyl)amine (**8**), 67%. TEA: triethylamine.

the importance of a serine residue that is close to the active site in the enzyme.

Results and Discussion

Synthesis, structures and solution properties of the model dinuclear copper(II) complex and the OPNO adduct

Synthesis: The unsymmetrical HBPMEP ligand (**9**) was synthesized according the procedure outlined in Scheme 2.^[17] For the introduction of the different coordination sites, the key step in the synthesis is realized by using synthon **4**.^[18] Substitution of the benzylic bromine group by *N,N*-bis(2-ethylpyridyl)amine (**5**) afforded **6**. After deprotection to form **7**, the hydroxymethyl group is chlorinated for alkylation with the second amine (amine **8**, which is different from the first one) to afford the desired ligand **9**.

The dibridged dinuclear copper(II) complex **3** was prepared by the addition of two equivalents of $\text{Cu}(\text{ClO}_4)_2 \cdot 6\text{H}_2\text{O}$ to a solution of the HBPMEP ligand in acetonitrile containing two equivalents of triethylamine (Scheme 2). The solid complex $[\text{Cu}_2(\text{BPMEP})(\mu\text{-OH})](\text{ClO}_4)_2$ (**3**) precipitated upon addition of tetrahydrofuran and green crystals of the compound suitable for X-ray single-crystal analysis were obtained by slow tetrahydrofuran diffusion into an acetonitrile solution of **3**. The reaction of complex **3** with 2.5 equivalents of HOPNO in methanol and slow vapor diffusion of diethyl ether afforded the resulting adduct $[\text{Cu}_2(\text{BPMEP})(\text{OPNO})]^{2+}$ (**10**²⁺) as a crystalline material.

Crystal structure descriptions of dications 3²⁺ and 10²⁺: All of the crystal structure parameters are given in the Experimental Section. The crystal of $[\text{Cu}_2(\text{BPMEP})(\mu\text{-OH})](\text{ClO}_4)_2 \cdot \text{THF}$ (**3**·THF; THF: tetrahydrofuran) contains one associated solvent molecule. An ORTEP view of the dica-

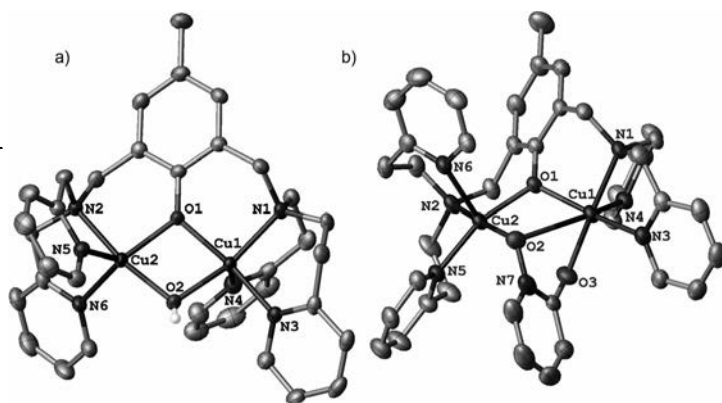


Figure 2. ORTEP plots of dications a) $[\text{Cu}_2(\text{BPMEP})(\mu\text{-OH})]^{2+}$ (**3**²⁺) and b) $[\text{Cu}_2(\text{BPMEP})(\text{OPNO})]^{2+}$ (**10a**²⁺). H atoms (except for the hydroxo group) and ClO_4^- counteranions were omitted for clarity. Ellipsoids are drawn at the 30% probability level.

tionic complex $[\text{Cu}_2(\text{BPMEP})(\mu\text{-OH})]^{2+}$ (**3**²⁺) is shown in Figure 2 A and selected bond lengths and angles are given in Table S1 in the Supporting Information.

The crystal structure reveals that the two copper atoms are doubly bridged by the phenoxo and a hydroxo group. The pentacoordination of the Cu1 and Cu2 atoms is achieved by the tertiary amine and two pyridine nitrogen atoms. However, the complex possesses geometrical unsymmetry because the environment around the Cu2 center is found to be intermediate between square pyramidal and trigonal bipyramidal ($\tau=0.53$),^[16] unlike that around the Cu1 center ($\tau=0.06$). The same dissymmetry exists in the enzyme (Table 1). In contrast, complexes **1** and **2** present similar coordination geometry for each copper center (two distorted trigonal bipyramids for **1** and two square pyramids for **2**).

Table 1. τ factors for copper sites in the *met* form of *S. castaneoglobisporus* Ty^[2a] (CuA, CuB) and complexes **1–3** (Cu1 and Cu2).

	CuA/Cu1	CuB/Cu2
<i>S. castaneoglobisporus</i> Ty <i>met</i> form	0.22	0.48
1	0.64	0.60
2	0.05	0.09
3	0.06	0.53

The Cu1–O1–Cu2 bond angle is 101.06(8) Å. The phenolate ring is slightly tilted toward the O1–O2 axis and twisted with respect to the O1–Cu2–O2–Cu1 plane. The Cu–O distances in the $[\text{Cu}_2\text{O}_2]$ unit are in the range of 1.8995–1.9876 Å and are slightly more asymmetric than those in **2** (1.928–1.961 Å). The four Cu1, Cu2, O1, and O2 atoms are in the same plane. The Cu1–O1–Cu2, Cu1–O2–Cu2, O1–Cu1–O2, and O1–Cu2–O2 angles are 101.0°, 104.6°, 76.8°, and 77.2°, respectively, which leads to the intermediate distance between Cu1 and Cu2 of 3.045 Å relative to those for **1** (2.966 Å) and **2** (3.077 Å).

The reaction of complex **3** with HOPNO in methanol and slow vapor diffusion of diethyl ether afforded compound **10**

as a crystalline material. The unit cell contains two crystallographically independent $[\text{Cu}_2(\text{BPMEP})(\text{OPNO})](\text{ClO}_4)_{2 \cdot 1/2}$ solvate entities, in which solvate stands for methanol and H_2O . Each cationic unit, one of which (**10a**²⁺) is shown in Figure 2 B (**10b**²⁺ is shown in Figure S1 in the Supporting Information), consists of two Cu^{II} atoms bridged by a phenoxo group and one deprotonated HOPNO molecule coordinated in an unsymmetrical bridging bidentate mode. Selected bond lengths and angles are reported in Table S2 in the Supporting Information and show no significant difference between the two copper dimers. The coordination sphere of each copper atom is completed by one amino and two pyridyl nitrogen atoms. Inside each dimer, the Cu atoms are separated by 3.242 Å in **10a** and 3.228 Å in **10b**. This distance, which is longer than in the dibridged (phenoxo and hydroxo) dicopper complex **3** (3.045 Å), is comparable with the one in **2-OPNO** (3.271 Å) but much shorter than that in adduct **1-OPNO** (3.927 Å).

The coordination polyhedrons around the Cu2 (in **10a**) and Cu4 (in **10b**) atoms are distorted square pyramids, the apical positions of which are occupied by the pyridine nitrogen atoms N6 and N13, respectively. The square plane is defined by the N2, N5, O1, and O3 atoms in **10a** (N9, N12, O4, and O5 in **10b**). The OPNO ligand is coordinated to Cu1 and Cu2 (or Cu3 and Cu4) in a bidentate mode. With the weak Cu1–O2 (or Cu3–O5) interaction (approximately 2.69 Å) taken into consideration, the coordination environment around Cu1 (or Cu3) forms a distorted octahedral geometry with the N1 (or N8) nitrogen atom of the tertiary amine, the N3 (or N10) pyridine nitrogen atom of the ligand, the O3 (or O6) oxygen atom from the OPNO ligand, and the O1 (or O4) atom of the phenoxo moiety in the equatorial coordination positions.

The axial coordination positions are occupied by the second oxygen atom (O2 or O5) from the OPNO ligand and the N4 (or N11) pyridine nitrogen atom. Angles involving the Cu atoms show deviation from the theoretical angles (the largest deviations in **10a** are encountered for O2–Cu1–N4 (149.0°, 31° deviation) and O1–Cu1–O2 (65.80°, 24.2° deviation)), which emphasizes the irregularity of the octahedron. The longer distances of the axial coordination (Cu1–O2: 2.695(2) Å for **10a**; Cu3–O5: 2.699(2) Å for **10b**; Cu1–N4: 2.207(2) Å for **10a**; Cu3–N11: 2.209(3) Å for **10b**) are evidence of a strong Jahn–Teller effect.

In the **1-OPNO** adduct, the OPNO ligand binds only one copper atom of the dinuclear site in a chelating mode, in contrast to the **2-OPNO** and **3-OPNO** (**10**) adducts, in which the bound OPNO ligand is in a bridging mode between the two copper(II) centers. The major difference between the **2-OPNO** and **10** adducts is the unsymmetrical coordination geometry around the copper centers. As a result, the coordination mode of the bound OPNO ligand resembles the expected coordination mode of the diphenol substrate on its way to product formation^[1b] or the proposed model from XAS studies of the Kojic acid adduct with *S. antibioticus* tyrosinase.^[11]

Solution studies: The ESI-MS spectrum of the **3-OPNO** (**10**) adduct provides two signals at m/z 894 ($z=1$) and 396.5 ($z=2$) for $[\text{Cu}_2(\text{BPMEP})(\text{OPNO})]^+(\text{ClO}_4)$ and $[\text{Cu}_2(\text{BPMEP})(\text{OPNO})]^{2+}$, respectively (Figure S2 in the Supporting Information). These data evidence that the dibridged dimeric copper(II) structure remains (in part) in solution, as already observed for adduct **2-OPNO**. The general UV/Vis features for dicopper(II) complex **3** in H_2O /dimethylsulfoxide (DMSO; 95/5) solution buffered at pH 7.0 with 50 mM 2-[4-(2-hydroxyethyl)-1-piperazinyl]ethanesulfonic acid (HEPES) are reported in Table 2 and can be compared with

Table 2. UV/Vis spectral data and binding constants for **3** and for adducts **1-OPNO**, **2-OPNO**, and **3-OPNO** (**10**).

	UV/Vis: λ_{max} [nm], (ϵ [$\text{M}^{-1}\text{cm}^{-1}$])		Binding constant (K_b) [M^{-1}]
	LMCT	d-d	
3 ^[a]	337 (1440) 386 (1220)	645 (200)	
1-OPNO ^[b,15]	430 (610)	700 (212)	440 ± 70
2-OPNO ^[b,15]	429 (5200)	670 (490)	8000 ± 400
3-OPNO ^[b]	420 (1530)	650 (170)	27100 ± 9750

[a] Determined at 25 °C from 2.7×10^{-4} M solution in H_2O /DMSO (95/5) buffered at pH 7 (HEPES, 50 mM). [b] Determined from the electronic spectra calculated from the refinement of absorbance data by the Specfit program.

the UV/Vis parameters determined from the calculated electronic spectra for all of the adducts from refinement of absorbance data by the Specfit program.^[19] All of the complexes are characterized by a ligand-to-metal charge-transfer (LMCT) transition between the bridging phenoxo group and the copper ions in the 300–450 nm region and a d–d transition in the 600–750 nm region (Table 2 and Figure S3 a and b in the Supporting Information).^[20]

The UV/Vis spectra of **3** are quite similar to those of **2** with a feature at 386 nm ($\epsilon \approx 1220 \text{ M}^{-1}\text{cm}^{-1}$), corresponding to the LMCT band maximum, a shoulder at 337 nm ($\epsilon \approx 1400 \text{ M}^{-1}\text{cm}^{-1}$), and a d–d band at 645 nm. Despite the difference in the geometry around the copper centers of **2** and **3** that was observed in the solid state, the similar d–d transition position could indicate geometrical changes in solution. Binding of HOPNO on complex **3** (Figure S4 in the Supporting Information) occurs with a shift of the absorption band at 386 nm up to 420 nm. The molar extinction coefficient is raised from 1220 to 1530 $\text{M}^{-1}\text{cm}^{-1}$. The d–d transition band at 645 nm ($\epsilon = 200 \text{ M}^{-1}\text{cm}^{-1}$) of **3** is slightly shifted to 650 nm ($\epsilon = 170 \text{ M}^{-1}\text{cm}^{-1}$), with a small decrease in the molar extinction coefficient. These data are reported in Table 2, together with the binding constants (K_b) of HOPNO to **1–3**, determined from the refinement of absorbance data versus the HOPNO concentration by the Specfit software. The series of curves exhibit an isobestic point, which indicates that one absorbing species is formed. The K_b value found with **3** is significantly higher than those obtained for complexes **2** and **1**, respectively,^[15] and the stoichiometry of the adduct is found to be 1:1. The UV/Vis spectrum from isolat-

ed **3**-OPNO (**10**; $2.7 \times 10^{-4} \text{ M}$) displays bands at 416 nm ($\epsilon \approx 1629 \text{ M}^{-1} \text{ cm}^{-1}$) and 649 nm ($\epsilon \approx 191 \text{ M}^{-1} \text{ cm}^{-1}$), values that are consistent with those obtained from the calculated electronic spectrum (Table 2).^[21]

EPR spectroscopy: The EPR spectra were measured at 100 K in a frozen solution in 1 mM H₂O/DMSO (1/1) buffered at pH 7 with 50 mM HEPES. Complex **3** is EPR silent, in accordance with the strong antiferromagnetic-coupling ($S=0$) ground spin state between the two copper atoms. This observation is consistent with the doubly bridged structure and the short Cu...Cu distance (3.045 Å) evidenced in the solid state. The EPR measurements for **10** in a frozen solution of DMSO/H₂O (1/1) at 100 K do not reveal the expected silent behavior for antiferromagnetic-coupled compounds, as with **3** or **2**-OPNO. The spectrum displays the presence of two sets of hyperfine lines from 220–400 mT, which suggests the overlap of two signals of uncoupled copper(II) ions (Figure S5 in the Supporting Information) that probably result from the dissociation of **10** in solution. A comparison with the spectrum of a solution of Cu(ClO₄)₂·6H₂O with two equivalents of HOPNO indicates that this corresponds to one of the signals observed in the spectrum of **10** (Figure S5 in the Supporting Information). These data show that some of the copper ions released from **10** in solution are complexed by HOPNO as a mononuclear species. Integration of the signal shows that 50% of the expected signal is recovered. This indicates that a magnetically coupled (EPR-silent) species is also present (adduct **10** in the solid state exhibits antiferromagnetic coupling between the copper ions; see below). Altogether, these data can be analyzed as evidence of changes in the copper coordination geometry after dissolution of **10** in a DMSO/H₂O (1/1) solution, so the observed EPR spectrum of **10** corresponds to a mixture of coupled and uncoupled species.

Catecholase activity: The catalytic activity of **3** in the oxidation of 3,5-di-*tert*-butylcatechol (3,5-DTBC) was studied in acetonitrile by monitoring the time dependence of the absorption of 3,5-di-*tert*-butylquinone (3,5-DTBQ) at 400 nm, which corresponds to the absorption of the product ($\epsilon = 1900 \text{ M}^{-1} \text{ cm}^{-1}$). The reactions follow a Michaelis–Menten behavior. The reaction rates are determined from the slope of the trace at 400 nm in the first 20 minutes of the reaction and a Lineweaver–Burk treatment gives a maximum velocity (V_{max}) of $1.2 \times 10^{-6} \text{ M}^{-1} \text{ s}^{-1}$ and a Michaelis constant (K_{M}) of 5 mM. After 90 min, a turnover number (TON) of 12 is observed, which is near the range of the values observed with complexes **1**^[14] and **2**^[15] (TON values of 16 and 18.3, respectively). Changes in geometry around the copper centers due to different pendant pyridine arms (with one or two carbon atoms) and unsymmetry are not critical for the catalytic efficiency of these complexes.

Magnetic properties and DFT calculations

The product of the magnetic susceptibility with temperature (χT) versus temperature plots for polycrystalline samples of **3** and **10** are given in Figure S6 in the Supporting Information. At room temperature, the χT values are much lower than the expected values for two magnetically independent Cu^{II} ions ($S=1/2$; $g=2$). Upon cooling, the values decrease rapidly and vanish at 75 K and 90 K for **3** and **10**, respectively. These behaviors suggest the presence of strong antiferromagnetic interactions between the two Cu^{II} ions and singlet states as the ground states. For **10**, this result in conjunction with the EPR spectrum in frozen solution highlights the difference of behavior mentioned before between the solid state and solution. Good fits of the experimental data with the equation given in the Experimental Section are obtained with $J = -210 \text{ cm}^{-1}$ and $g = 2.4$ for **3** and $J = -225 \text{ cm}^{-1}$ and $g = 2.23$ for **10**. No intermolecular interactions are considered.

The electronic structures of dinuclear copper(II) complexes remain a theoretical challenge due to the difficulty of providing an accurate description of electron correlation effects for these systems.^[22] In this case, the size of the systems suggests the use of density functional methods. The approximation was made that the triplet and singlet state geometries are close and all geometries have been determined from a triplet state. Selected structural parameters for complex **3** are listed in Table S1 in the Supporting Information. As for complexes **1** and **2**,^[15] a good agreement between calculated and experimental data is obtained and confirms that our approximation is correct. The computed values of the J exchange coupling for complexes **1–3**, calculated by using a broken symmetry approach,^[23] are -136 , -636 , and -394 cm^{-1} , respectively. These results are supported by experimental magnetic measurements. The determined J value for **1** is -112 cm^{-1} ,^[14] for **2** is $< -300 \text{ cm}^{-1}$,^[15] and for **3** is -210 cm^{-1} in this work. Analysis of the [Cu₂O₂] core geometries explains this order. From Table 3, it can be observed that the values of the Cu–O–Cu angles for **3** are intermediate with those values for **1** and **2**, in correlation with their J values.

Table 3. Calculated exchange coupling constants (J [cm⁻¹]) and Cu–O–Cu angles [°] for complexes **1–3** (B3LYP/6-311g*^[a]).

	J	Cu–O–Cu	Cu–O(H)–Cu
1	-136 (-112) ^[14]	95.7	102.1
3	-394 (-210)	101.0	104.7
2	-636 (< -300) ^[15]	103.7	105.5

[a] Values in parenthesis correspond to experimental values.

Calculations were also done for the complexes formed with HOPNO. Selected structural parameters for **10** (**3**-OPNO) are listed in Table S2 in the Supporting Information. A good agreement between the calculated and experimental data is also obtained. The OPNO ligand bridges the two copper atoms in a bidentate mode, as for **2**-OPNO, but the symmetrical coordination of **2**-OPNO around the copper atoms is lost in **10**. The computed value of the J ex-

change coupling for **3**-OPNO (**10**) is -291 cm^{-1} , which is in agreement with the experimental data given above (-225 cm^{-1}). This value is slightly smaller than that of **2**-OPNO, computed to be -391 cm^{-1} .^[15] This can be explained by the small decrease in the Cu–O–Cu angle if we compare **10** with **2**-OPNO. The value of the Cu–O–Cu angle is 114.2° for **10** and 115.5° for **2**-OPNO. Relative to those in **2** and **3**, the two Cu atoms for the OPNO complex are less coupled. Figure 3 represents the magnetic orbitals of **10** and **3**. The exchange interaction passes essentially through the oxygen atom of the Cu–O–Cu bridge; the exchange path is broken through the OPNO ligand. This is not the case for **2** and **3**, in which a path is developed on the $[\text{Cu}_2\text{O}_2]$ core.

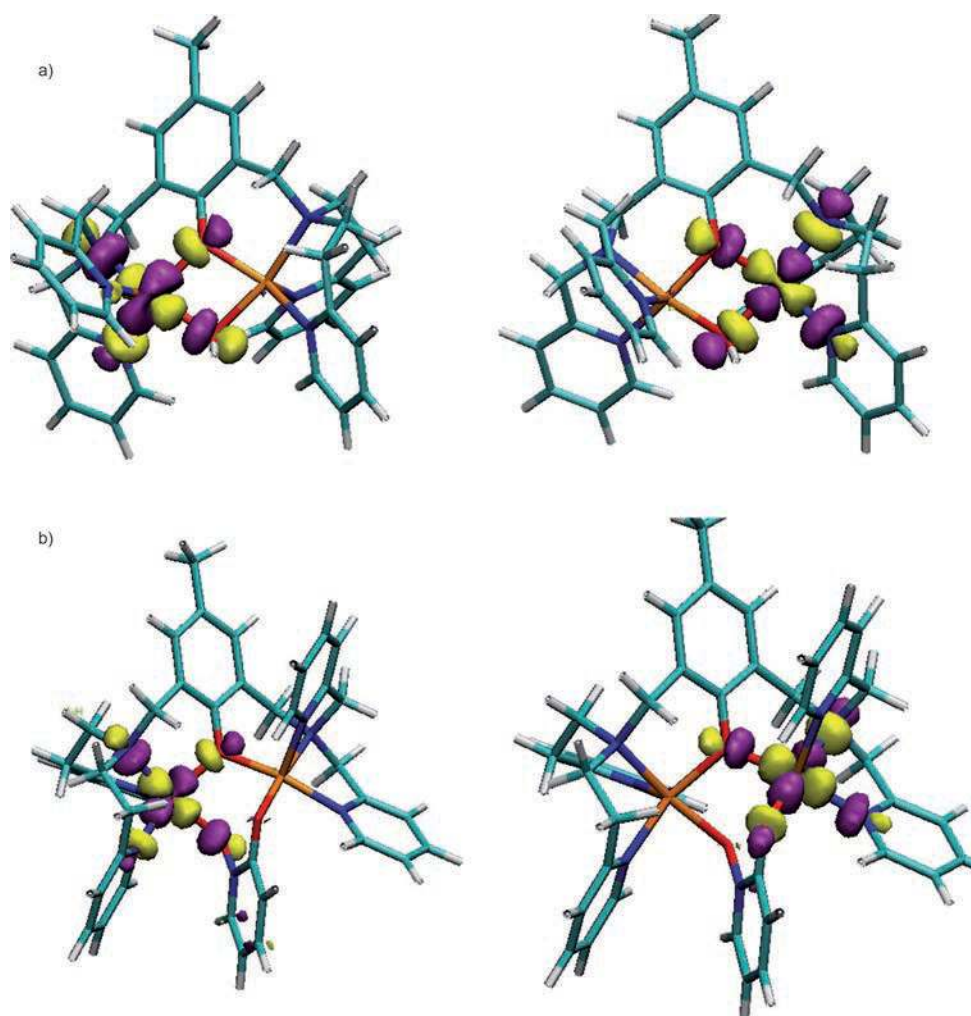


Figure 3. Magnetic orbitals for the broken-symmetry state of a) **3** and b) **10**.

Binding studies on the enzyme

HOPNO has already been described as a competitive inhibitor in the oxidation of *L*-3,4-dihydroxyphenylalanine (*L*-DOPA) catalyzed by mushroom Ty (IC_{50} value of $1.2\ \mu\text{M}$ and inhibition constant (K_I) of $1.8\ \mu\text{M}$).^[10] We confirmed that

HOPNO is also a competitive inhibitor for the bacterial Ty from *S. antibioticus*. Indeed, *S. antibioticus* Ty inhibition by HOPNO is concentration dependent with an IC_{50} value estimated to be $(6.4 \pm 1.1)\ \mu\text{M}$ ($[\text{L-DOPA}] = 0.175\ \text{mM}$; Figure S7 in the Supporting Information) and it exhibits the kinetic features of competitive inhibition ($K_I = (7.7 \pm 0.2)\ \mu\text{M}$; Figure S8 and S9 in the Supporting Information) with efficiency comparable to the mushroom Ty form.

To calculate the binding mode of deprotonated HOPNO in the enzyme, the optimized geometries obtained for OPNO complexes were used as starting points for the placement of the inhibitor into the active pocket of the enzyme. The construction of the initial geometry of these complexes is detailed in the Experimental Section. Geometry optimizations were done on triplet states, with the assumption that the spin state doesn't change considerably the geometry of the active state, as observed in model complexes. The same minimum was obtained if the optimized geometry for **2**-OPNO or **3**-OPNO was used; thus, only two minima between the OPNO ligand and the bacterial Ty were obtained. They can be seen in Figure 4 and distances between the ligand and the copper atoms of the active site are listed in Table S3 in the Supporting Information.

In the first structure (Figure 4A), the OPNO ligand bridges the two copper atoms as in **2**-OPNO and **3**-OPNO. The intermetallic distance from Cu1...Cu2 is close to the distance obtained for the optimized geometries of **2**-OPNO and **3**-OPNO ($3.32\ \text{\AA}$ for the bacterial Ty and **2**-OPNO, $3.36\ \text{\AA}$ for **3**-OPNO). As in **3**-OPNO, the binding mode is unsymmetrical. The distance between the oxygen atom of the nitrosyl group and one copper atom is $1.98\ \text{\AA}$, whereas the distance between the oxygen atom of the hydroxy group and the other copper atom is $2.11\ \text{\AA}$.

For bacterial Ty, this is explained by the presence of a serine group, Ser260, close to the active site, which can form a hydrogen bond with the oxygen atom of the OPNO ligand linked to Cu2 (see Figure 4A). This interaction also explains the structure of the second minimum obtained for the enzyme (Figure 4B). From the chelating mode of **1**-OPNO,

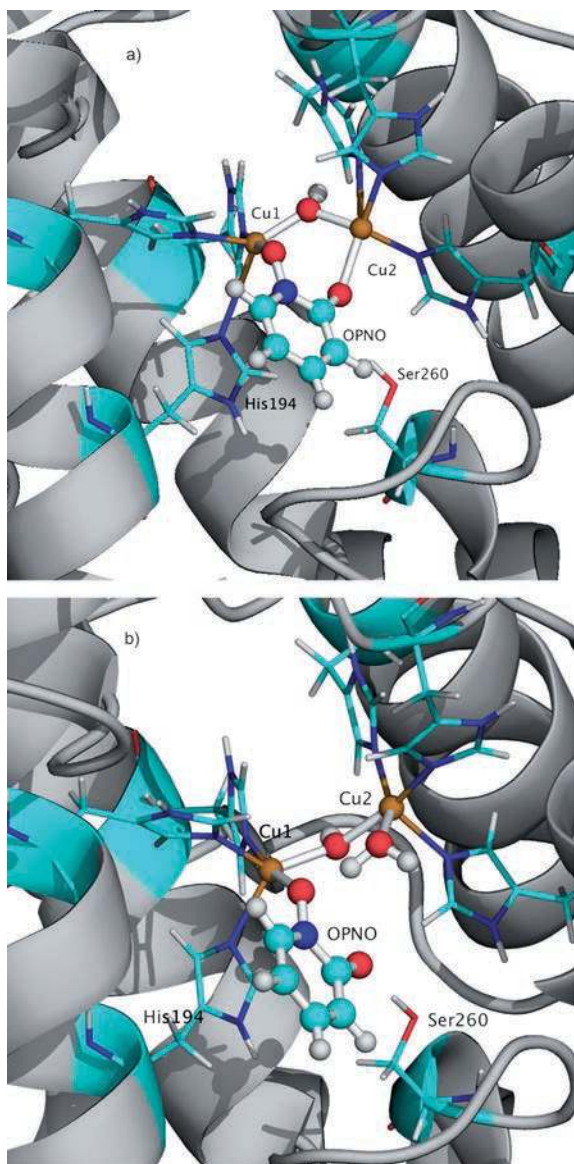


Figure 4. QM/MM optimized complexes between bacterial Ty and the OPNO ligand. Two binding modes are obtained: a) a bridging mode; b) a monodentate mode. The ligand, the copper atoms, and the hydroxo group bridging the two copper atoms are displayed as balls and sticks. Copper atoms are shown in orange.

the ligand shifted during the optimization geometry to give a hydrogen bond between the oxygen atom of the hydroxy group of the OPNO ligand and Ser260. In this case, the coordination between the Cu2 atom and the oxygen atom is broken and the binding mode becomes monodentate.

For the two binding modes in the enzyme, the aromatic ring of the OPNO ligand is π stacked with His194 of the enzyme. Figure 4 illustrates this interaction for the two structures. The distances between the OPNO ligand and His194 are similar in the two structures, which suggests an interaction of the same strength. This interaction was already observed in the crystallographic structures of type-3 copper enzymes. For example, it was found between the in-

hibitor phenylthiourea (PTU) and a histidine residue close to the active site of a catechol oxidase (PDB code: 1BUG).^[24]

To compare the two binding modes, we can look at the QM/MM energy of the system. However, the monodentate mode (Figure 4B) has an extra water molecule on the free copper atoms of the active site. So, a single-point calculation has been performed for the monodentate mode without the water molecule. This mode was found to be favorable by $9.8 \text{ kcal mol}^{-1}$. This comparison indicates that the OPNO ligand prefers to be coordinated to only one copper atom, as we found previously for the dinuclear copper(II) complex $[\text{Cu}_2(\text{BPMP})(\mu\text{-OH})](\text{ClO}_4)_2$. For the copper complex, this coordination is explained by the rigidity of the chelate ring that forms the complex. In the enzyme, it should be explained by the steric constraints imposed by the environment. However, different approximations are introduced in this comparison, for example, the need to perform certain statistical simulations to obtain average structures and energies for the enzyme. Thus, this comparison can be seen as a first approach.

Conclusion

An understanding of the different parameters that control the binding mode of transition-state analogue inhibitors of Ty is an important step to unravel the structural features that govern tyrosinase activity. HOPNO is an efficient competitive inhibitor of mushroom and bacterial tyrosinases. From a series of dicopper(II) complexes based on different lengths of the pyridine side arms, diverse OPNO adducts have been described (chelating, bridging). In this article, we present the binding mode found on a new Ty functional model. The latter involves two different complexing arms (namely (bis(2-ethylpyridyl)amino)methyl and (bis(2-methylpyridyl)amino)methyl) designed to tune an unsymmetrical binding of the OPNO ligand. These variations in binding modes were used as starting points to study the binding mode of the OPNO ligand in the enzyme. QM/MM calculations suggest that the OPNO ligand coordinated to only one copper atom in the enzyme, as in the most rigid complex **1**. However, one hydrogen bond between the ligand and a serine residue close to the active site changes considerably the binding mode in the enzyme compared to that in **1**. This result highlights the importance of the second coordination sphere in the enzyme.

Experimental Section

General: All starting materials were commercially available and used as purchased, unless stated. ESI mass spectra were recorded on an Esquire 300 plus Bruker Daltonis instrument. Elemental analyses were performed at the analysis facilities of the Department of Chemistry of the University of Grenoble, France. UV/Vis absorption spectra were obtained by using a Varian Cary 50 spectrophotometer operating in the 200–1000 nm range with quartz cells. The temperature was maintained at 25°C with a tem-

perature-control unit. ^1H NMR data were recorded on a Bruker Advance 300 spectrometer at 323 K with the deuterated solvent as a lock. X-band EPR spectra were recorded at 100 K with a Bruker ESP EMX Plus spectrometer equipped with a nitrogen-flow cryostat and operating at 9.3 GHz (X band).

Safety note: Although no problems were encountered during the preparation of the perchlorate salts, suitable care should be taken when handling such potentially hazardous compounds.

Enzymatic assays: The *S. antibioticus* tyrosinase activity was checked with spectroscopic methods by using L-DOPA as a substrate. HOPNO was dissolved in a 10% DMSO stock solution. Phosphate buffer (pH 7.0) was used to dilute the DMSO stock solution of the compounds. *S. antibioticus* tyrosinase (1 mL; 4.5 U mL^{-1}) was first preincubated with the compounds in 50 mM phosphate buffer (pH 7.0) for 5 min at 25°C . The L-DOPA was then added to the reaction mixture and the enzyme reaction was monitored by measuring the change in absorbance at 475 nm of the DOPACHrome product for 5 min.

Synthesis: The binucleating ligand HBPEMP was prepared by the method described in the Supporting Information.

Complex 3: A solution of $\text{Cu}(\text{ClO}_4)_2 \cdot 6\text{H}_2\text{O}$ (470 mg; 1.26 mmol) in CH_3CN (10 mL) was added dropwise to HBPEMP (312 mg; 0.56 mmol) dissolved in CH_3CN (15 mL). The initial yellow solution turned dark green. Et_3N (160 μL ; 1.12 mmol) was then added and the solution was stirred for 3 h at room temperature. The solvent was partially removed under reduced pressure and a few drops of THF were added. The resulting solution (10 mL) was allowed to stand for 3 days at -20°C . A green powder (256 mg) was collected by filtration (yield: 51%). Crystals of X-ray quality were obtained by vapor diffusion of THF in a solution of **3** in CH_3CN . The crystalline material, if crushed and exposed to air, loses some of the noncoordinated THF; UV/Vis (in HEPES (pH 7.0, 50 mM), DMSO (5%)): λ_{max} (ϵ) = 390 (1380), 650 nm ($180 \text{ M}^{-1} \text{ cm}^{-1}$); ESI-MS: m/z : $z=1$, 801.1 [$M + \text{H}^+ - \text{ClO}_4^-$]; $z=2$, 350.1 [$M + \text{H}^+ - 2 \text{ClO}_4^-$]; elemental analysis: calcd (%) for $\text{C}_{35}\text{H}_{38}\text{Cl}_2\text{Cu}_2\text{N}_6\text{O}_{10} \cdot 0.5 \text{C}_4\text{H}_8\text{O}$: C 47.44, H 4.62, N 8.79; found: C 47.37, H 4.07, N 8.14.

Complex 10: A solution of HOPNO (15.7 mg, 2.5 equiv) in methanol (2 mL) was added to a solution of complex **3** (40 mg, 0.44 mM) in methanol (10 mL) and a small amount of acetone. The brown solution was stirred for 30 min. A slow diffusion of diethyl ether into the methanolic solution provided **10** as a suitable crystal for X-ray analysis. The crystalline material, if crushed and exposed to air, loses the noncoordinated solvent; ESI-MS: m/z : $z=1$, 894.1 [$M - \text{ClO}_4^-$]; $z=2$, 396.5 [$M - 2 \text{ClO}_4^-$]; UV/Vis (in HEPES (pH 7, 50 mM), DMSO (5%)): λ_{max} (ϵ) = 420 (1530), 630 nm ($200 \text{ M}^{-1} \text{ cm}^{-1}$); elemental analysis: calcd (%) for $\text{C}_{40}\text{H}_{41}\text{Cl}_2\text{Cu}_2\text{N}_7\text{O}_{11}$: C 48.34, H 4.16, N 9.87; found: C 48.70, H 4.20, N 9.83.

Determination of stability constants: The binding constants of the inhibitor to the dinuclear Cu^{II} complexes were determined by spectrophotometric titration in water/DMSO (95/5) solutions buffered at pH 7.0 with 50 mM HEPES. The titrations were carried out by adding small aliquots of a concentrate solution of the inhibitor to solutions of the complexes. The spectral data were refined with the Specfit program.^[19]

Catechol oxidase activity and kinetics: UV/Vis spectra and kinetics were recorded by using a quartz cuvette (1.0 cm) and a Varian Cary 50 UV/Vis spectrophotometer equipped with a Peltier thermostating accessory. The kinetics of the 3,5-DTBC oxidation was determined by the initial-rates method by monitoring the increase in the product (3,5-DTBO) at 400 nm. All of the kinetic experiments were conducted at a constant temperature of 25°C , monitored with a thermostat. A $4.8 \times 10^{-5} \text{ M}$ solution of the complex with 3,5-DTBC (100 equiv) was used and the solution was saturated with dioxygen (1 atm). Under these conditions, catechol was not oxidized without the copper complexes. The measurements were performed in CH_3CN . Under these conditions, no changes were observed from the initial solutions of the complexes (UV/Vis spectrophotometry). The kinetics parameters were determined for a $4.8 \times 10^{-5} \text{ M}$ solution of complex **3** and 0.96–44.8 mM solutions of the substrate.

Crystal structure determination and refinement: Single crystals of complexes **3**-THF and **10**-solvate were mounted on a Kappa CCD Nonius diffractometer equipped with graphite-monochromated $\text{Mo}_{\text{K}\alpha}$ radiation ($\lambda = 0.71073 \text{ \AA}$) at 200 K. The reflections were corrected for Lorentz and polarization effects and for absorption by using the SADABS program.^[25] The data were then integrated and scaled with EvalCCD software.^[26] The structures were solved by direct methods and refined by full-matrix least-square methods with the SHELXL program^[27] implemented in Olex2 software.^[28] For both structures, all non-hydrogen atoms were refined with anisotropic thermal parameters. Hydrogen atoms were generated in idealized positions, riding on the carrier atoms, with isotropic thermal parameters, except for the hydrogen atom of the hydroxy group, which was localized on a difference Fourier map and was added. Pertinent crystallographic data and refinement details are summarized in Table 4. CCDC 881633 (**3**-THF) and CCDC 881634 (**10**-solvate) contain the supplementary crystallographic data for this paper. These data can be obtained free of charge from the Cambridge Crystallographic Data Centre via www.ccdc.cam.ac.uk/data_request/cif.

Magnetic measurements: Magnetic susceptibility data (2–300 K) were collected on powdered samples by using a SQUID magnetometer from

Table 4. Crystallographic data for **3** and **10**.

	3	10
formula	$[\text{Cu}_2(\text{C}_{35}\text{H}_{38}\text{N}_6\text{O}_2)](\text{ClO}_4)_2 \cdot \text{THF}$	$2[\text{Cu}_2(\text{C}_{40}\text{H}_{41}\text{N}_7\text{O}_3)](\text{ClO}_4)_2 \cdot 0.85 \text{ MeOH} \cdot 0.15 \text{ H}_2\text{O}$
M_{w}	972.80	2017.15
color and morphology	green rectangular prism	brown plate
crystal size [mm]	$0.39 \times 0.18 \times 0.14$	$0.4 \times 0.22 \times 0.1$
crystal system	monoclinic	triclinic
space group	$P1\ 21/c\ 1$	$P\bar{1}$
a [\AA]	12.899(2)	12.5531(16)
b [\AA]	30.5659(10)	18.427(4)
c [\AA]	10.394(3)	19.109(3)
α [$^\circ$]	90.00	99.903(11)
β [$^\circ$]	95.054(8)	101.645(11)
γ [$^\circ$]	90.00	95.829(13)
V [\AA^3]	4082.4(13)	4221.9(12)
ρ [g cm^{-3}]	1.583	1.587
T [K]	200.0	200.0
Z	4	2
μ [mm^{-1}]	1.240	1.205
total	46213	57438
reflns		
unique	8436	16230
reflns		
observed	6506 ($F > 2\sigma$)	11882 ($F > 2\sigma$)
reflns		
R_{int}	0.0377	0.0447
$R^{\text{[a]}}$	0.0356	0.0434
$R(w)^{\text{[a]}}$	0.0763	0.0896
GOF	1.031	1.061
$\Delta\rho_{\text{min}}/\Delta\rho_{\text{max}}$ [e \AA^{-3}]	$-0.505/0.611$	$-0.447/0.535$

[a] Refinement based on F if $w = 1/[\sigma^2(F_o) + (0.03499P)^2 + 3.5696P]$ for **3**-THF and $w = 1/[\sigma^2(F_o) + (0.0366P)^2 + 6.1205P]$ for **10** and with $P = (Fo^2 + 2Fc^2)/3$.

Quantum Design (model MPMS-XL) in a 0.1 T applied magnetic field. All data were corrected for the contribution of the sample holder and diamagnetism of the samples estimated from Pascal's constants.^[29] The magnetic exchange interactions (J) were extracted by simulation of the magnetic susceptibility by considering the spin Hamiltonian $H = -2S_1S_2$ ($S_i = 1/2$) and by using Equation (1) in which J is the exchange interaction parameter, T the temperature, β the Bohr magneton, k the Boltzmann's constant, g the Landé g -factor and N the Avogadro's number.^[29b]

$$\chi T = \frac{Ng^2\beta^2}{k[3 + \exp(-2J/kT)]} \quad (1)$$

QM and QM/MM calculations: QM calculations were based on DFT and have been performed with the Gaussian03 package.^[30] Full geometry optimizations were carried out by using the hybrid functional B3LYP^[31] and the 6-31g* basis set on all atoms.^[32] All geometry optimizations were done on a triplet state. The Yamaguchi formula^[33] was used to estimate the exchange coupling constants. For that purpose, additional single-point high-spin (HS) and broken-symmetry (BS) calculations were done on the previously optimized geometries with the same B3LYP functional and a larger basis set (6-311g* for Cu and coordinating O atoms, 6-31g* for all remaining atoms).

QM/MM calculations were performed by using the Gaussian03 package for the QM part and Tinker 4.2^[34] for the MM part. Both mechanical and electrostatic embedding (direct polarization) schemes were used to describe interactions between the QM and MM part, thus ensuring a good description of the effects of the environment on the active site. The QM part contains the two copper atoms, the hydroxy group, the side chains of the six histidine residues linked to the copper atoms in the met form, the ligand, and an extra water molecule for the chelating mode. All MM atoms belonging to residues within a distance of 4 Å of the QM part were allowed to relax during geometry optimizations and the remaining structure was kept frozen. All QM/MM geometry optimizations were carried with a triplet state. The partition between the QM and MM parts has led to the cut of the six C α -C β bonds of the histidine residues in the active site. These dangling bonds have been described as strictly localized bonding orbitals (SLBO's) within the local self-consistent field (SCF)^[35] methodology. In this scheme, SLBO's remain frozen during the SCF procedure. A detailed description of the SLBO's and parameters can be found in the Supporting Information and related references. The QM part was treated at the B3LYP/6-31g* level of theory and the MM part was described with the Amber 99SB force field^[36] for the protein and TIP3P for the solvent. The initial structure for the enzyme is based on the crystal structure of the bacterial tyrosinase complexed with the ORF38 caddie protein (PDB code: 2AHK).^[2a] The caddie protein and the water molecules, with the exception of three water molecules close to the active site, were removed. The addition of H atoms leads to the protonation of all histidines on the δ nitrogen atom, whereas the aspartate and glutamate residues remain deprotonated and the arginine and lysine residues are positively charged. The system was first solvated with a truncated octahedral box of TIP3PBOX water molecules (10 Å radius) and neutralized with one Na⁺ ion. For the first energy minimization, the Amber99SB force field was used in conjunction with specific parameters developed for copper ions, histidine residues, and the hydroxy group linked to the copper atoms in the active site. These parameters are given in the Supporting Information and are based on the force field developed by Comba and Remenyi^[37] for blue copper proteins. The system was energy minimized for 3000 steepest descent steps followed by 12000 conjugated gradient steps. No constraints were applied in order to allow complete relaxation of the system. The QM optimized structures of **1**-OPNO, **2**-OPNO, and **3**-OPNO were then aligned with the active site of the enzyme with the 'fit atom' tool of Sybyl version 8.0.^[38] Alignment was done between the His Ne and Cu atoms from the enzyme and the N and Cu atoms of the OPNO complexes. Some atoms of the complexes were then introduced into the enzyme pocket to replace the copper atom and hydroxy group of the met Ty form. Figure S10 in the Supporting Information illustrates the introduction of the OPNO complexes into the enzyme structure. Once the relaxed structure was obtained, QM/MM geometry optimizations were performed.

Acknowledgements

The authors thank the French Agence Nationale pour la Recherche for financial support (ANR-09-BLAN-0028-01/02) and for grants to C.B. and C.D. We are grateful to Florian Molton (DCM) for measuring EPR spectra. This work has been carried out in the framework of COST action CM1003 (WG 2) and of Labex ARCANE.

- [1] a) R. H. Holm, P. Kennepohl, E. I. Solomon, *Chem. Rev.* **1996**, *96*, 2239–2314; b) M. Rolff, J. Schottenheim, H. Decker, F. Tuzcek, *Chem. Soc. Rev.* **2011**, *40*, 4077–4098; c) A. W. J. W. Tepper, E. Lonardi, L. Bubacco, G. W. Canters in *Handbook of metalloproteins* (Ed.: A. Messerschmidt), John Wiley, Chichester, **2010**, DOI: 10.1002/0470028637.met0470028265.
- [2] a) Y. Matoba, T. Kumagai, A. Yamamoto, H. Yoshitsu, M. Sugiyama, *J. Biol. Chem.* **2006**, *281*, 8981–8990; b) M. Sendovski, M. Kanteev, V. Shuster Ben-Yosef, N. Adir, A. Fishman, *J. Mol. Biol.* **2011**, *405*, 227–237.
- [3] B. Albolmaali, H. Taylor, U. Weser in *Bioinorganic chemistry*, 91st ed. (Eds.: J. G. M. Clarke, C. Jorgensen, D. Mingos, G. Palmer, P. Sadler, R. Weiss, R. Willimans), Springer, Berlin/Heidelberg, **1998**, pp. 91–190.
- [4] H. S. Mason, *J. Biol. Chem.* **1948**, *172*, 83–99.
- [5] a) V. N. Sehgal, G. Srivastava, *Int. J. Dermatol.* **2008**, *47*, 1041–1050; b) R. E. Boissy, J. J. Nordlund, *Pigment Cell Res.* **1997**, *10*, 12–24.
- [6] C. Visús, R. Andres, J. I. Mayordomo, M. J. Martinez-Lorenzo, L. Murillo, B. Saez-Gutierrez, C. Diestre, I. Marcos, P. Astier, F. J. Godino, F. J. Carapeto-Marquez de Prado, L. Larrad, A. Tres, *Melanoma Res.* **2007**, *17*, 83–89.
- [7] Y. Xu, A. H. Stokes, W. M. Freeman, S. C. Kumer, B. A. Vogt, K. E. Vrana, *Mol. Brain Res.* **1997**, *45*, 159–162.
- [8] T. S. Chang, *Int. J. Mol. Sci.* **2009**, *10*, 2440–2475.
- [9] a) J. S. Chen, C. Wei, M. R. Marshall, *J. Agric. Food Chem.* **1991**, *39*, 1897–1901; b) R. C. Hider, K. Lerch, *Biochem. J.* **1989**, *257*, 289–290.
- [10] E. Peyroux, W. Ghattas, R. Hardré, M. Giorgi, B. Faure, A. J. Simaan, C. Belle, M. Réglier, *Inorg. Chem.* **2009**, *48*, 10874–10876.
- [11] L. Bubacco, R. Spinazze, S. della Longa, M. Benfatto, *Arch. Biochem. Biophys.* **2007**, *465*, 320–327.
- [12] W. T. Ismaya, H. J. Rozeboom, A. Weijn, J. J. Mes, F. Fusetti, H. J. Wichers, B. W. Dijkstra, *Biochemistry* **2011**, *50*, 5477–5486.
- [13] a) K. D. Karlin, Y. Gultneth, T. Nicholson, J. Zubieta, *Inorg. Chem.* **1985**, *24*, 3725–3727; b) H. Börzel, P. Comba, H. Pritzkow, *Chem. Commun.* **2001**, 97–98; c) J. Ackermann, F. Meyer, E. Kaifer, H. Pritzkow, *Chem. Eur. J.* **2002**, *8*, 247–258.
- [14] S. Torelli, C. Belle, I. Gautier Luneau, J. L. Pierre, E. Saint Aman, J. M. Latour, L. Le Pape, D. Luneau, *Inorg. Chem.* **2000**, *39*, 3526–3536.
- [15] M. Orio, C. Bochot, C. Dubois, G. Gellon, R. Hardré, H. Jamet, D. Luneau, C. Philouze, M. Réglier, G. Serratrice, C. Belle, *Chem. Eur. J.* **2011**, *17*, 13482–13494.
- [16] A. W. Addison, T. N. Rao, J. Reedijk, J. van Rijn, G. Verschoor, *J. Chem. Soc. Dalton Trans.* **1984**, 1349–1356.
- [17] During the redaction of this manuscript, synthesis of this ligand by a different method has been published: F. Heims, V. Mereacre, A. Ciancetta, S. Mebs, A. K. Powell, C. Greco, K. Ray, *Eur. J. Inorg. Chem.* **2012**, 4565–4569.
- [18] C. Belle, G. Gellon, C. Scheer, J. L. Pierre, *Tetrahedron Lett.* **1994**, *35*, 7019–7022.
- [19] a) H. Gampp, M. Maeder, C. J. Meyer, A. D. Zuberbühler, *Talanta* **1985**, *32*, 95–101; b) H. Gampp, M. Maeder, C. J. Meyer, A. D. Zuberbühler, *Talanta* **1985**, *32*, 257–264; c) H. Gampp, M. Maeder, C. J. Meyer, A. D. Zuberbühler, *Talanta* **1986**, *33*, 943–951.
- [20] B. J. Hathaway, *Struct. Bonding (Berlin)* **1984**, *57*, 55–118.
- [21] Although UV/Vis data have not been obtained under the same experimental conditions (H₂O/DMSO ratio, concentration) as those of the EPR experiments, we cannot rule out instability of the **3**-OPNO adduct with a small release of copper in solution, as observed in

- EPR experiments (and not observed for **1-OPNO** and **2-OPNO**). Thus, data from UV/Vis experiments for **10** should be considered with this possible event taken into account.
- [22] B. F. Gherman, C. J. Cramer, *Coord. Chem. Rev.* **2009**, *253*, 723–753.
- [23] a) L. Noodleman, *J. Chem. Phys.* **1981**, *74*, 5737–5743; b) L. Noodleman, D. A. Case, *Adv. Inorg. Chem.* **1992**, *38*, 423–470; c) L. Noodleman, E. R. Davidson, *Chem. Phys.* **1986**, *109*, 131–143.
- [24] T. Klabunde, C. Eicken, J. C. Sacchettini, B. Krebs, *Nat. Struct. Biol.* **1998**, *5*, 1084–1090.
- [25] SADABS v2.10, Program for empirical absorption correction of area detector data, G. M. Sheldrick, University of Göttingen, Germany, **2003**.
- [26] A. J. M. Duisenberg, L. M. J. Kroon-Batenburg, M. M. Schreurs, *J. Appl. Crystallogr.* **2003**, *36*, 220–229.
- [27] G. M. Sheldrick, *Acta Crystallogr.* **2008**, *A64*, 112–122.
- [28] O. V. Dolomanov, L. J. Bourhis, R. J. Gildea, J. A. K. Howard, H. Puschmann, *J. Appl. Crystallogr.* **2009**, *42*, 339–341.
- [29] a) J. M. Pascal, *Ann. Chim. Phys.* **1910**, *19*, 5–69; b) O. Kahn, *Molecular Magnetism*, VCH, Weinheim, **1993**.
- [30] Gaussian 03, revision A.1., M. J. Frisch, G. W. Trucks, H. B. Schlegel, G. E. Scuseria, M. A. Robb, J. R. Cheeseman, V. G. Zakrzewski, J. A. Montgomery, J. R. E. Stratmann, J. C. Burant, S. Dapprich, J. M. Millam, A. D. Daniels, K. N. Kudin, M. C. Strain, O. Farkas, J. Tomasi, V. Barone, M. Cossi, R. Cammi, B. Mennucci, C. Pomelli, C. Adamo, S. Clifford, J. Ochterski, G. Petersson, A. P. Y. Ayala, Q. Cui, K. Morokuma, D. K. Malick, A. D. Rabuck, K. Raghavachari, J. B. Foresman, J. Cioslowski, J. V. Ortiz, A. G. Baboul, B. B. Stefanov, G. Liu, A. Liashenko, P. Piskorz, I. Komaromi, R. Gomperts, R. L. Martin, D. J. Fox, T. Keith, M. A. Al-Laham, C. Y. Peng, A. Nanayakkara, M. Challacombe, P. M. W. Gill, B. Johnson, W. Chen, M. W. Wong, J. L. Andres, C. Gonzalez, M. Head-Gordon, J. A. Pople, Gaussian, Inc., Pittsburg, PA, **2003**.
- [31] a) A. D. Becke, *J. Chem. Phys.* **1993**, *98*, 5648–5652; b) C. Lee, W. Yang, R. C. Parr, *Phys. Rev. B* **1988**, *37*, 785–789; c) K. Yamaguchi, F. Jensen, A. Dorigo, K. N. Houk, *Chem. Phys. Lett.* **1988**, *149*, 537–542.
- [32] a) P. C. Hariharan, J. A. Pople, *Theor. Chim. Acta* **1973**, *28*, 213–222; b) P. C. Hariharan, J. A. Pople, *Mol. Phys.* **1974**, *27*, 209–214.
- [33] a) T. Soda, Y. Kitagawa, V. Onishi, Y. Tanaka, Y. Shigeta, H. Nagao, Y. Yoshioka, K. Yamaguchi, *Chem. Phys. Lett.* **2000**, *319*, 223–230.
- [34] Tinker, 4.2 ed., J. W. Ponder, Washington University, Saint Louis, MO, **2004**.
- [35] a) X. Assfeld, J. L. Rivail, *Chem. Phys. Lett.* **1996**, *263*, 100–106; b) N. Ferré, J. L. Rivail, X. Assfeld, *J. Comp. Chem.* **2002**, *23*, 610–624.
- [36] J. Wang, P. Cieplak, P. A. Kollman, *J. Comp. Chem.* **2000**, *21*, 1049–1074.
- [37] P. Comba, R. Remenyi, *J. Comp. Chem.* **2002**, *23*, 697–705.
- [38] SYBYL 8.0, Tripos Associates, Inc., Saint Louis, MO, **2007**.